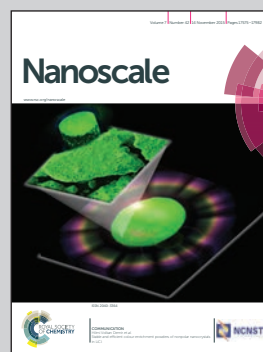**Showcasing collaborative research from the Department of Chemistry and Biochemistry of the University of Bern, the Department of Chemistry of the University of Fribourg, Switzerland and the Department of Applied Chemistry of Chou University, Japan.**

Title: Layer-by-layer grown scalable redox-active ruthenium-based molecular multilayer thin films for electrochemical applications and beyond

A layer-by-layer assembly method to prepare redox-active ruthenium based molecular multilayer thin films with well controlled thicknesses was developed. The fine control of the physicochemical properties at the nanometer scale, with excellent stability of the layers under ambient conditions, makes the multilayer coatings of this type an excellent material for energy storage, energy conversion and molecular electronics applications.

ROYAL SOCIETY OF CHEMISTRY

www.rsc.org/nanoscale

Layer-by-layer grown scalable redox-active ruthenium-based molecular multilayer thin films for electrochemical applications and beyond†

Veerabhadrarao Kaliginedi,*[a] Hiroaki Ozawa,[b] Akiyoshi Kuzume,*[a]
Sivarajakumar Maharajan,[c] Ilya V. Pobelov,[a] Nam Hee Kwon,[c] Miklos Mohos,[a]
Peter Broekmann,[a] Katharina M. Fromm,*[c] Masa-aki Haga*[b] and
Thomas Wandlowski‡[a]

Here we report the first study on the electrochemical energy storage application of a surface-immobilized ruthenium complex multilayer thin film with anion storage capability. We employed a novel dinuclear ruthenium complex with tetrapodal anchoring groups to build well-ordered redox-active multilayer coatings on an indium tin oxide (ITO) surface using a layer-by-layer self-assembly process. Cyclic voltammetry (CV), UV-Visible (UV-Vis) and Raman spectroscopy showed a linear increase of peak current, absorbance and Raman intensities, respectively with the number of layers. These results indicate the formation of well-ordered multilayers of the ruthenium complex on ITO, which is further supported by the X-ray photoelectron spectroscopy analysis. The thickness of the layers can be controlled with nanometer precision. In particular, the thickest layer studied (65 molecular layers and approx. 120 nm thick) demonstrated fast electrochemical oxidation/reduction, indicating a very low attenuation of the charge transfer within the multilayer. *In situ*-UV-Vis and resonance Raman spectroscopy results demonstrated the reversible electrochromic/redox behavior of the ruthenium complex multilayered films on ITO with respect to the electrode potential, which is an ideal prerequisite for *e.g.* smart electrochemical energy storage applications. Galvanostatic charge–discharge experiments demonstrated a pseudocapacitor behavior of the multilayer film with a good specific capacitance of 92.2 F g^{-1} at a current density of 10 μA cm^{-2} and an excellent cycling stability. As demonstrated in our prototypical experiments, the fine control of physico-chemical properties at nanometer scale, relatively good stability of layers under ambient conditions makes the multilayer coatings of this type an excellent material for *e.g.* electrochemical energy storage, as inter-layers in inverted bulk heterojunction solar cell applications and as functional components in molecular electronics applications.

[a]Department of Chemistry and Biochemistry, University of Bern, Freiestrasse 3, CH-3012 Bern, Switzerland. E-mail: kaliginedi@dcb.unibe.ch, akiyoshi.kuzume@dcb.unibe.ch
[b]Department of Applied Chemistry, Faculty of Science and Engineering, Chuo University, Bunkyo-ku, Tokyo 112-8551, Japan. E-mail: mhaga@kc.chuo-u.ac.jp
[c]Department of Chemistry, University of Fribourg, Chemin du Musée 9, CH-1700 Fribourg, Switzerland. E-mail: katharina.fromm@unifr.ch
†Electronic supplementary information (ESI) available: Synthesis of [Ru$_2$(tppz)(LPOH)$_2$](PF$_6$)$_4$; cyclic voltammetry in aqueous electrolyte; EQCM, AFM, UV-Vis and resonance Raman spectroscopy results; data analysis details are presented in ESI. See DOI: 10.1039/c5nr04087f
‡Deceased on 27.06.2015.

Introduction

Recent developments in portable consumer electronics, such as transparent and/or flexible electronic devices and integrated microsystems, demand next generation energy storage devices, which must meet the requirements of high performance (rapid charge/discharge) and high stability (low performance loss) during the charging–discharging cycles as well as low cost.[1–5] Conventional electrochemical energy storage devices, such as batteries, are known to suffer from slow charge–discharge rates and difficulties in maintaining their efficiency upon scaling-down in size.[1,6] This creates a strong demand for small, flexible, high performance and low cost portable energy storage solutions.[4,7–12]

It was suggested that electrochemical supercapacitors, which store the electric energy by charging the electric double layer, may suit this purpose. Electrochemical supercapacitors based on graphene[7,13–15] and/or carbon nanotubes[3,4,16–18] exhibit higher power densities, faster charge/discharge and longer cycling stability than conventional batteries. However,

the practical use of carbon based supercapacitors is limited by their low charge storage capacities.[4] The gap between conventional batteries and supercapacitors[12] is bridged by electrochemical pseudocapacitors,[4] which accumulate charge in the bulk of a redox-active material during a fast oxidation/reduction reaction. To date, electrochemical pseudocapacitors based on conducting polymers,[19] covalent organic frameworks,[20] as well as transition metal oxides[4,21] and their composites[5,22–28] have been proposed. Pseudocapacitors employing thin films of transition metal oxides and their composites show very high capacitance, but suffer from low electric conductance and inefficient mass transport as well as from high material costs.[27,29] Highly-conductive, flexible and transparent films of conducting polymers can be easily formed by spin coating or (electro)chemical polymerization, but it is challenging to ensure their efficient binding to the conductive support and to control their morphology (thickness, porosity). As a result, pseudocapacitors based on conducting polymers often display poor cycling stability.[19]

A better alternative to traditional conducting polymers for many applications is represented by coordination networks formed by redox-active metal organic frameworks and/or covalent organic frameworks.[20,30,31] The structure of coordination networks can be designed according to the desired functionality by a careful selection of metal centers and functional ligands. Different research groups demonstrated various applications of metal coordination network films, for example as interlayers for efficient inverted bulk heterojunction solar cells[32] and photocurrent generation,[33] as active layers in electrochromic devices,[34,35] integrated molecular logic[36] and memory[37] applications.

Metal coordination network films are highly conductive and exhibit nanopores which allow a good contact between the electrolyte and the metal ions inside the film, thus facilitating their oxidation/reduction.[31] Although these properties render them particularly suitable for energy storage applications, systematic studies exploring the redox-active porous coordination polymers on electrode surfaces with this goal are still scarce.[30,31] Facile, low cost, and environmentally friendly materials with improved stability are desired to enable better integration of coordination networks with electrodes for their practical energy storage applications. To address some of the aforementioned issues, we report here the first study on the energy storage application of surface-immobilized ruthenium complex multilayer thin films with anion storage capability, whose properties can be tuned as a function of film thickness.

Experimental

Materials

$[Ru_2(tppz)(LPOH)_2](PF_6)_4$ (Ru–N) was synthesized according to the synthetic methodology (ESI section 1†). All solutions were prepared from Milli-Q water (18.2 MΩ cm, total organic carbon < 4 ppb), CH_3CN (Sigma Aldrich), $ZrOCl_2 \cdot 8H_2O$ (Sigma Aldrich), $HClO_4$ (Merck). ITO coated glass samples (Kuramoto Co., Ltd)

cut to 0.5 cm × 0.5 cm squares were cleaned by heating to 80 °C in 5 : 1 : 1 (v : v : v) H_2O–H_2O_2–NH_3 solution for 1 h, then washed with a copious amount of Milli-Q water.

Assembly of multilayer film of Ru–N on ITO

3.07 mg of Ru–N was dissolved in 5 ml of Milli-Q water by adding 3 drops of the 25% ammonia solution upon sonication. The pH of the solution was adjusted to 6 by the addition of 0.1% HCl while monitoring the pH with a pH meter. Then the solution was transferred to a volumetric flask and the volume was adjusted to 20 ml by adding Milli-Q water to obtain a 50 μM solution of Ru–N. Each Ru–N monolayer was assembled either on a bare or modified ITO sample by immersing the sample into the 50 μM Ru–N solution for 3 h. The Ru–N monolayers were connected by Zr(IV) ions by immersing the sample into a 20 mM aqueous solution of $ZrOCl_2$ for 30 min. After each assembly step, the sample was washed by immersing three times into a beaker filled with Milli-Q water (exchanged after each sample immersion) and dried under an Ar flow. The Ru–N/Zr assembly cycles were repeated until the desired number of layers, respectively thickness of the multilayer film was achieved (Fig. 1).

Cyclic voltammetry

Cyclic voltammograms were measured in a lab-made single compartment glass cell at room temperature in solutions deoxygenated by Ar and under Ar atmosphere. All cyclic voltammetry and spectroelectrochemical measurements employed a lab-built potentiostat; platinum wires were used as counter and quasi-reference electrodes. The potential of the platinum quasi-reference electrode was calibrated as −100 ± 10 mV vs. the equilibrium potential of the ferrocenium/ferrocene redox pair used as an internal standard and it is also calibrated as +765 ± 10 mV vs. $Ag/AgNO_3$ reference electrode.

UV-Vis and Raman spectroscopy

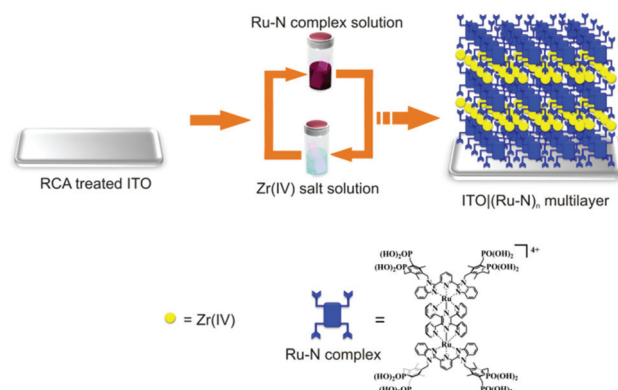A Cary 5E UV-Vis-NIR spectrometer was employed for UV-Vis spectroscopy. LabRAM HR800 confocal Raman microscope

Fig. 1 Layer-by-layer assembly of $[Ru_2(tppz)(LPOH)_2](PF_6)_4$ multilayers on ITO substrate. (RCA stands for Radio Corporation of America (RCA) treatment).[55]

(Horiba Jobin Yvon) was employed for Raman spectroscopy. *In situ* UV-Vis and Raman spectroelectrochemical measurements were carried out in Ar-deaerated 0.1 M HClO$_4$ in CH$_3$CN using a custom-made optical quartz cell under a continuous Ar flow above the solution. For Raman spectroscopy we employed a long-working-distance objective lens (50 times magnification, 8 mm focal length) with a numerical aperture of 0.1 to focus DPSS laser (excitation wavelength 532 nm, power 1 mW) on the sample. The Raman signal was collected in a backscattering geometry.

Ex situ X-ray photoelectron spectroscopy

Ex situ X-ray photoelectron spectra of ITO|(Ru–N)$_n$ multilayer samples were measured by using a Shimadzu/Kratos Axis HSi spectrometer with monochromated Al Kα radiation as an excitation source.

Galvanostatic charge/discharge measurements

Charging/discharging curves and capacitances of ITO|(Ru–N)$_{65}$ were measured in Ar-deaerated 0.1 M HClO$_4$ in CH$_3$CN with Arbin 2000 battery test instrument using a three electrode cell and under a continuous Ar flow above the solution.

Results and discussion

Layer-by-layer assembly of ruthenium complex multilayer ITO|(Ru–N)$_n$

The multilayer thin films were prepared with the novel redox-active dinuclear ruthenium complex [Ru$_2$(tppz)(LPOH)$_2$](PF$_6$)$_4$ (Ru–N) on an indium tin oxide (ITO) substrate employing an aqueous-based layer-by-layer (LBL) assembly process (Fig. 1). After immobilization of the primer layer of Ru–N on the ITO, this involves bidentate/tridentate binding through P–O–In and/or P–O–Sn bonds.[38–42] Then the substrate was immersed in the solution containing Zr(IV) ions, resulting in the formation of Zr-phosphonate linkage with Ru–N in the primer layer. During the assembly process two Ru–N layers were connected by successive reaction of Zr(IV) ions with phosphonate linker groups through R–P(O)O$_2$–Zr–O$_2$P(O)–R bond, a concept developed by Mallouk *et al.* and others.[43–49] A similar assembly strategy has been applied for the fabrication of multilayers used in the implementation of high-*k* gate dielectrics for low-voltage organic field effect transistors,[50] thin film transistors[51,52] and molecular electronics applications.[53,54] We describe the structure of the multilayers as ITO|(Ru–N)$_n$, where "*n*" represents the number of Ru–N layers.

Ex situ characterization of ruthenium complex multilayers

To gain more insight into the structure and composition of the multilayers, we monitored the layer-by-layer growth of the ITO|(Ru–N)$_n$ multilayer film with *ex situ* UV-Vis, Raman spectroscopy, X-ray photoelectron spectroscopy (XPS). Two growth mechanisms, namely linear and exponential growth, have been reported for the multilayer films assembled by LBL procedures in the literature.[22,56–61]

Fig. 2a shows the *ex situ* UV-Vis absorption spectra of ITO|(Ru–N)$_n$ with *n* = 1–65. The UV-Vis absorption spectra feature two bands. The band observed in the visible region (576 nm) corresponds to the metal to ligand charge transfer (MLCT) and the one in the UV region (357 nm) corresponds to intraligand ππ* transitions. Similar UV-Vis transitions for the basic backbone structure of Ru–N were also reported by Nagashima *et al.*[62] With an increasing number of layers, the integrated absorbance of the MLCT band at 576 nm increased linearly without any shift in peak position up to 65 layers (Fig. 2b). Similar observations were also reported by Shinomiya *et al.*[63] and van der Boom *et al.*,[64] where the plots of absorbance *vs.* the number of immersion cycles exhibited a linear relationship, indicating linear growth of a layered Pd-based network.

The *ex situ* Raman spectra of the ITO|(Ru–N)$_n$ films with different amount of assembled layers (Fig. 2c and d) also show a linear increase of the Raman signal intensities of Ru–N with *n*. The layer thickness extracted from AFM scratching profiles increases linearly with *n* with a slope from which a thickness of 1.9 nm per layer can be derived. This value is very close to the length of Ru–N calculated from the molecular modeling (Fig. S5†). Additionally, *ex situ* AFM images of bare ITO and of the thickest multilayer (*n* = 65, estimated thickness 123 nm) show surface structures with comparable roughness (Fig. S3†).

Additionally, to get a clear insight into the layer composition we also monitored *ex situ* XPS spectra for ITO|(Ru–N)$_n$ (*n* = 1–13) multilayer film growth (Fig. 3 and S12†). The signal intensities for the O 1s, Sn 3d, In 3d, In 4s peaks from the ITO substrate were gradually decreased with increasing the ITO|(Ru–N)$_n$ layer thickness. On the other hand, the signal intensi-
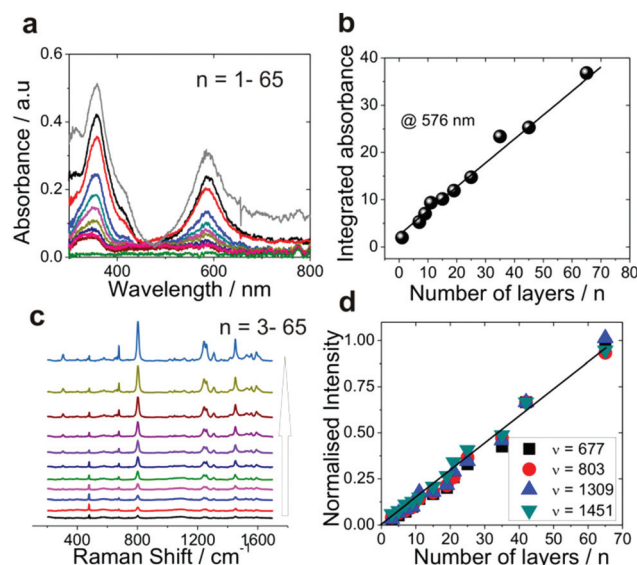

Fig. 2 *Ex situ* spectroscopy of ITO|(Ru–N)$_n$ multilayers. (a) UV-Vis absorption spectroscopy, *n* = 1–65. (b) Integrated absorbance of the 576 nm band *versus n*. (c) Raman spectroscopy, *n* = 3, 5, 7, 9, 11, 15, 19, 21, 25, 35, 42, 65. (d) Normalized intensity of Raman signals at ν = 667 cm^{-1}, 803 cm^{-1}, 1309 cm^{-1} and 1457 cm^{-1} *vs. n*.
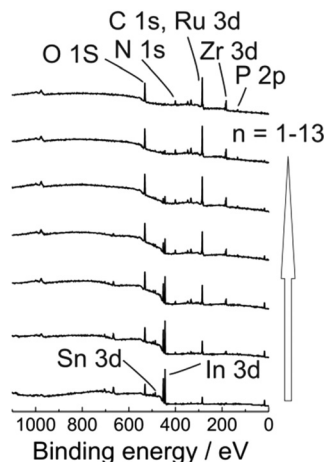
Fig. 3 *Ex situ* XPS spectra of ITO|(Ru–N)$_n$ (n = 1, 3, 5, 7, 9, 11, 13) multilayers.

ties for N 1s, C 1s, Ru 3d, P 2p peaks were increased with increasing the thickness of the ITO|(Ru–N)$_n$ layers. Presence of Ru 3d signals confirmed the "+2" oxidation state of the ruthenium center in the multilayer film.[65] No Zr 3d signals were observed for bare ITO and n = 1 sample. While clear Zr 3d signals were observed from bilayers (n = 2) and other successive multilayers, confirming the Zr ion incorporation into the layers (Fig. 3 and S12†). Combining and comparing the results of *ex situ* UV-Vis, *ex situ* Raman spectroscopy, *ex situ* XPS, *ex situ* AFM strongly indicate a uniform and linear growth of the multilayers of Ru–N on ITO.

Cyclic voltammetry

Cyclic voltammograms of ITO|(Ru–N)$_n$ in 0.1 M HClO$_4$ in CH$_3$CN (Fig. 4) show two reversible redox peaks corresponding to the oxidation of Ru(II)–Ru(II) to Ru(III)–Ru(II) and of Ru(III)–Ru(II) to Ru(III)–Ru(III). To avoid the degradation of ITO|(Ru–N)$_n$ multilayer films, the potential was always cycled between −0.25 to 0.7 V *vs.* Pt quasi-reference electrode. The total integrated charge obtained from cyclic voltammetry experiments increases linearly with the number of layers giving the slope of 12×10^{-6} C cm^{-2} per layer (Fig. 4b), which is equivalent to the
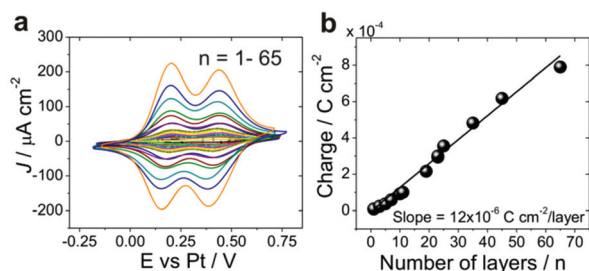
charge of one full Ru–N monolayer (ESI section 2†). This indicates the addition of one full monolayer at each step of the layer-by-layer assembly and further confirms the formation of uniform multilayer films. The total integrated charge shows no saturation with the increase of layer thickness up to 65 layers. Moreover, the cyclic voltammogram of ITO|(Ru–N)$_{65}$ display well-defined reversible redox peaks even at a scan rate of 100 mV s^{-1}. This indicates the high accessibility of the redox-active ruthenium ions for the electrolyte.[19,47,54,66] Similar results were also obtained in 0.1 M aqueous HClO$_4$ (ESI section 2†).

Spectroelectrochemistry

The electrochemical reversibility and structural changes in ITO|(Ru–N)$_n$ multilayers during the redox transitions were investigated by employing *in situ* UV-Vis and Raman spectroelectrochemical experiments as well as electrochemical quartz crystal microbalance (EQCM) experiments (ESI section 3†). The results of UV-Vis spectroelectrochemistry (ESI section 5†) and data reported by Nagashima *et al.*[62] show clear spectral changes due to the two well-separated one-electron redox processes which occurred in the multilayer, resulting in the formation of three dinuclear ruthenium complex with different oxidation states: Ru(II)–Ru(II), Ru(II)–Ru(III), and Ru(III)–Ru(III). Fig. 5 displays the potential dependent Raman spectra of ITO|(Ru–N)$_{65}$ in 0.1 M HClO$_4$ in CH$_3$CN. These data clearly indicate a reversible structural reorganization with respect to the applied electrode potential (details of the peak intensity changes and assignment of peaks are shown in the ESI section 5†). These observations are further supported by the EQCM data (ESI section 3†), which clearly demonstrated a reversible mass increase during the oxidation of the multilayer. We attribute this to the penetration of ClO$_4^-$ anions into the coordination network, which is required to support the charge balance during the oxidation of Ru(II) to Ru(III). Similar mass changes at the electrode surface accompanying electrochemical processes were also reported by Shinomiya *et al.* and other groups.[63,67] The observed reversible electrochromic/redox behavior and structural change of the ITO|(Ru–N)$_n$ film with
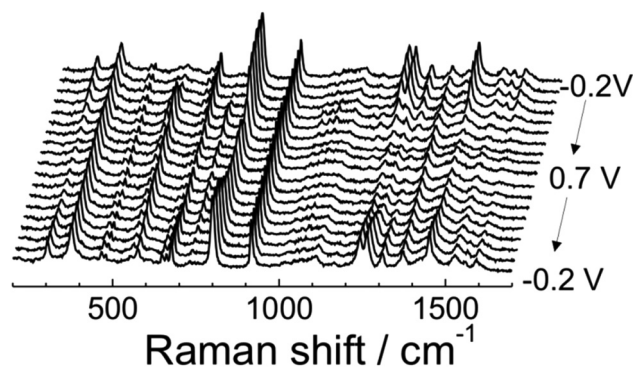

Fig. 4 Cyclic voltammetry of ITO|(Ru–N)$_n$ multilayers. (a) Cyclic voltammograms in 0.1 M HClO$_4$ in CH$_3$CN, n = 1–65, scan rate 100 mV s^{-1}. (b) Total integrated charge from curves in panel (A) *vs. n*.

Fig. 5 Potential dependent Raman spectra of ITO|(Ru–N)$_{65}$ on the ITO surface in 0.1 M HClO$_4$ in CH$_3$CN.

respect to the electrode potential is an ideal characteristic of functional materials that can be employed for electrochemical sensors, smart energy storage devices and molecular electronics applications.[4]

Characterisation of the ruthenium complex multilayer ITO|(Ru–N)$_{65}$ in an electrochemical energy storage application

Further we present a proof of principle application of ITO|(Ru–N)$_{65}$ multilayer for electrochemical energy storage. The charging of the ITO|(Ru–N)$_{65}$ electrode was first characterized by cyclic voltammetry in 0.1 M HClO$_4$ in CH$_3$CN (Fig. 6a). The separation between respective oxidation and reduction peaks (Fig. 6b) is close to 25 mV for the two lowest scan rates, 10 and 50 mV s^{-1}. Theoretically, the oxidation and reduction peaks for a surface-confined redox-active species should be completely symmetric for a very fast charging or for very low potential scan rates. However, the residual hysteresis is rather small and constant at the low scan rate limit, and we attribute it to the imperfect potential distribution in the electrochemical cell and/or to a rather high resistance of the CH$_3$CN-based solution. The kinetic limitations due to the slow mass transfer manifest themselves as an increase of the peak to peak separation at scan rates above 100 mV s^{-1} (Fig. 6b). A specific capacitance of 95.3 F g^{-1} was obtained for the ITO|(Ru–N)$_{65}$ multilayer from the voltammograms measured at 10 mV s^{-1} and is close to those reported for pseudocapacitors based on vertically aligned carbon nanotubes (70–120 F g^{-1}),[68–70] covalent organic frameworks (48 ± 10 F g^{-1})[20] and conducting

polymers (75–530 F g^{-1}).[19,66] It decreases to 81.8 F g^{-1} at 100 mV s^{-1} and further by approximately 20% when the scan rate increases by one order of magnitude (Fig. 6c). This decrease, however, is quite small compared to that found for conducting polymers,[19] metal oxide materials[21] and their composite electrodes.[4,19,25] We attribute the fast oxidation/reduction of the multilayer to two factors: (I) fast diffusion of the anions into and out of the multilayer film during the redox reaction, preventing kinetic limitations due to the slow charge compensation; and (II) fast charge transport within the multilayer itself, which might be due to the charge transfer mechanisms specific for the electrochemical environment. The long range electron transfer[53,71] in Ru–N multilayers is currently a subject of further studies.

The stability of ITO|(Ru–N)$_{65}$ was characterized by continuous potential cycling with the rate of 100 mV s^{-1} (Fig. 6d). The capacitance retention after 2000 cycles was 80%, which is much higher than reported for the most conducting polymer based devices.[19,72,73] We also assayed the stability of these layers stored under ambient conditions (Fig. S11A†) and also the sample heated on a hot plate at 150 °C (in air) by employing the cyclic voltammetry (Fig.S11B, ESI section 6†). These results clearly demonstrated the excellent stability of ruthenium complex multilayer films under ambient conditions and reasonably good stability with the sample heated at 150 °C. However a small change in the charge was observed in case of sample heated on a hot plate at 150 °C for 30 minutes, which is may be due to a small material loss or surface oxidation during heating.

To characterize the charge/discharge properties of the ruthenium complex multilayer electrodes under standardized conditions, we further carried out galvanostatic charge–discharge experiments upon application of a constant current density varied from 10 to 100 µA cm^{-2} (Fig. 7a). Based on these curves, the electrodes display pseudocapacitor behaviour of ITO|(Ru–N)$_{65}$ with two small plateaus at 0.12 V and 0.37 V vs. Pt. These plateaus correspond to the reversible Faradaic reactions associated with the oxidation/reduction of the two ruthenium ions in the complex (cf. Fig. 4a and 6a). Similar electrochemical pseudocapacitor behaviour of conducting polymers (polyaniline, polypyrrole, PEDOT, polythiophene, etc.),[19] transition metal oxides (RuO$_2$, MnO$_2$, V$_2$O$_5$, Fe$_2$O$_3$, etc.),[21] hydroxides (Ni(OH)$_2$)[74,75] and their composites has been reported in the literature.[4,5,76] For our electrodes, an excellent capacitance retention of ≈100% was observed after 10 cycles at all applied current densities (Fig. 7b). A maximum capacitance of 92.2 and 63.3 F g^{-1} was found for the smallest (10 µA cm^{-2}) and the highest (100 µA cm^{-2}) applied current density (Fig. 7c). Although the decrease of the capacitance with increasing current density is due to the diffusion limitations, it is much lower than for the other systems with only 35% at one order of magnitude increase in current density. This again indicates fast charge transfer kinetics upon the electrochemical oxidation/reduction of the multilayer.

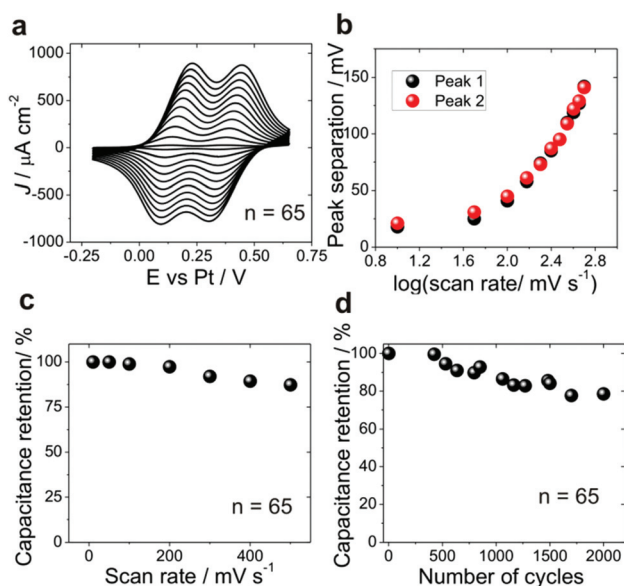The insert in Fig. 7c displays the Ragone plot (energy density vs. power density) of ITO|(Ru–N)$_{65}$ (ESI section 8†).

Fig. 6 Charging and stability test of ITO|(Ru–N)$_{65}$. (a) Cyclic voltammograms in 0.1 M HClO$_4$ in CH$_3$CN, scan rate 10 to 500 mV s^{-1}. (b) Peak to peak separation vs. logarithm of the scan rate for the curves in panel (a). (c) Specific capacitance calculated from the curves in panel (a) as a function of the scan rate. (d) Capacitance retention as a function of cycle number for ruthenium complex multilayer (n = 65) electrode at 100 mV s^{-1}.
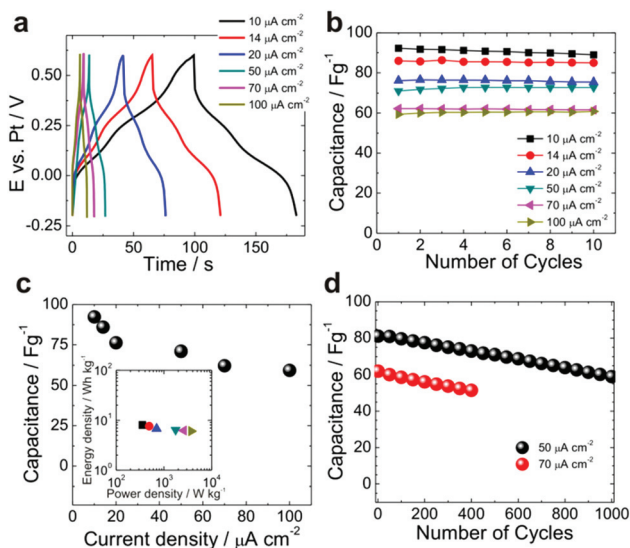
Fig. 7 Galvanostatic charge–discharge experiments with $ITO|(Ru-N)_{65}$. (a) Galvanostatic charge and discharge curves in 0.1 M $HClO_4$ in CH_3CN. (b) Specific capacitance *vs.* the cycle number. (c) Specific capacitance at different current densities; insert shows the Ragone plot. (d) Capacitance retention *vs.* the cycle number at current densities of 50 µA cm^{-2} and 70 µA cm^{-2}.

Our ruthenium complex multilayer electrode delivered a maximum power density of ~3736 W kg^{-1} with an energy density of ~6 W h kg^{-1}, as obtained for the characterized potential range of 0.9 V. We note that in order to achieve a larger operating voltage range and increase the energy and power density of multilayer-based supercapacitors, it is highly desirable to couple such electrodes with suitable counter electrodes.[4,19,77] The cycling stability of the electrode was also tested over 1000 galvanostatic charge–discharge cycles (Fig. 7d). At 50 µA cm^{-2}, a capacitance retention of 72% was found. A similar trend was observed for higher current density of 70 µA cm^{-2} for 400 cycles (Fig. 7d).

Conclusions

We successfully demonstrated the assembly of coordination networks based on a novel redox-active dinuclear ruthenium complex into multilayers on an ITO substrate. The multilayers were produced by a simple yet effective layer-by-layer assembly from an aqueous solution and are characterized by the well-defined orientation of the molecules, leading to a uniform growth. The thickness of the coating and the charge stored scale both with the number of layers assembled. The latter are limited only by the available assembly time, respectively deposition cycles. Even the thickest coating with 65 molecular layers demonstrates fast electrochemical oxidation/reduction. Without further device optimization, this multilayer exhibited an excellent performance and stability upon thousands of charging/discharging cycles in a prototypical energy storage

application. Our results show that redox-active coordination networks grown on conductive substrates have a potential to unfold into a new class of promising materials for electrochemical energy storage as well as for other applications.

The assembly procedure adopted in this study allows multilayer formation on various other oxide materials (Indium tin oxide, fluorine doped tin oxide, quartz/glass, sapphire *etc.*). The characteristics of the fabricated multilayers indicate that coordination networks of this type are promising materials for energy storage as well as for many other applications: as an effective linker between electrode and bacteria in microbial fuel cells[78–80] or as interlayers in organic photovoltaic devices,[81–83] for nanoelectronic devices with electrochemically-controlled charge transport properties,[84,85] or for fundamental studies of the long range electron transfer,[86] to mention only a few.

References

1   J. M. Tarascon and M. Armand, *Nature*, 2001, **414**, 359–367.
2   M. S. Whittingham, *Chem. Rev.*, 2004, **104**, 4271–4301.
3   P. M. Ajayan and O. Z. Zhou, *Carbon Nanotubes*, 2001, **80**, 391–425.
4   P. Simon and Y. Gogotsi, *Nat. Mater.*, 2008, **7**, 845–854.
5   C. Liu, F. Li, L.-P. Ma and H.-M. Cheng, *Adv. Mater.*, 2010, **22**, E28–E62.
6   A. Patil, V. Patil, D. W. Shin, J.-W. Choi, D.-S. Paik and S.-J. Yoon, *Mater. Res. Bull.*, 2008, **43**, 1913–1942.
7   K. S. Kim, Y. Zhao, H. Jang, S. Y. Lee, J. M. Kim, J. H. Ahn, P. Kim, J. Y. Choi and B. H. Hong, *Nature*, 2009, **457**, 706–710.
8   L. Zhao, Y. X. Xu, T. F. Qiu, L. J. Zhi and G. Q. Shi, *Electrochim. Acta*, 2009, **55**, 491–497.
9   Q. Wu, Y. X. Xu, Z. Y. Yao, A. R. Liu and G. Q. Shi, *ACS Nano*, 2010, **4**, 1963–1970.
10 D. Deng and J. Y. Lee, *Chem. Mater.*, 2008, **20**, 1841–1846.
11 Y.-G. Guo, J.-S. Hu and L.-J. Wan, *Adv. Mater.*, 2008, **20**, 2878–2887.

12 S. W. Lee, B. M. Gallant, H. R. Byon, P. T. Hammond and Y. Shao-Horn, *Energy Environ. Sci.*, 2011, **4**, 1972–1985.

13 Y. W. Zhu, S. Murali, W. W. Cai, X. S. Li, J. W. Suk, J. R. Potts and R. S. Ruoff, *Adv. Mater.*, 2010, **22**, 3906–3924.

14 Y. Zhu, S. Murali, M. D. Stoller, K. J. Ganesh, W. Cai, P. J. Ferreira, A. Pirkle, R. M. Wallace, K. A. Cychosz, M. Thommes, D. Su, E. A. Stach and R. S. Ruoff, *Science*, 2011, **332**, 1537–1541.

15 Y. Wang, Z. Shi, Y. Huang, Y. Ma, C. Wang, M. Chen and Y. Chen, *J. Phys. Chem. C*, 2009, **113**, 13103–13107.

16 E. Frackowiak and F. Beguin, *Carbon*, 2001, **39**, 937–950.

17 E. Frackowiak, K. Metenier, V. Bertagna and F. Beguin, *Appl. Phys. Lett.*, 2000, **77**, 2421–2423.

18 D. N. Futaba, K. Hata, T. Yamada, T. Hiraoka, Y. Hayamizu, Y. Kakudate, O. Tanaike, H. Hatori, M. Yumura and S. Iijima, *Nat. Mater.*, 2006, **5**, 987–994.

19 G. A. Snook, P. Kao and A. S. Best, *J. Power Sources*, 2011, **196**, 1–12.

20 C. R. DeBlase, K. E. Silberstein, T. Thanh-Tam, H. D. Abruna and W. R. Dichtel, *J. Am. Chem. Soc.*, 2013, **135**, 16821–16824.

21 C. D. Lokhande, D. P. Dubal and O.-S. Joo, *Curr. Appl. Phys.*, 2011, **11**, 255–270.

22 L. Shao, J.-W. Jeon and J. L. Lutkenhaus, *Chem. Mater.*, 2012, **24**, 181–189.

23 X. Zhang, W. Yang and D. G. Evans, *J. Power Sources*, 2008, **184**, 695–700.

24 Y. G. Wang and X. G. Zhang, *Electrochim. Acta*, 2004, **49**, 1957–1962.

25 M. N. Hyder, B. M. Gallant, N. J. Shah, Y. Shao-Horn and P. T. Hammond, *Nano Lett.*, 2013, **13**, 4610–4619.

26 M. N. Hyder, S. W. Lee, F. C. Cebeci, D. J. Schmidt, Y. Shao-Horn and P. T. Hammond, *ACS Nano*, 2011, **5**, 8552–8561.

27 P. Yang, Y. Ding, Z. Lin, Z. Chen, Y. Li, P. Qiang, M. Ebrahimi, W. Mai, C. P. Wong and Z. L. Wang, *Nano Lett.*, 2014, **14**, 731–736.

28 P. Yang, X. Xiao, Y. Li, Y. Ding, P. Qiang, X. Tan, W. Mai, Z. Lin, W. Wu, T. Li, H. Jin, P. Liu, J. Zhou, C. P. Wong and Z. L. Wang, *ACS Nano*, 2013, **7**, 2617–2626.

29 X. Zhang, W. Shi, J. Zhu, D. J. Kharistal, W. Zhao, B. S. Lalia, H. H. Hng and Q. Yan, *ACS Nano*, 2011, **5**, 5280–5280.

30 S.-L. Li and Q. Xu, *Energy Environ. Sci.*, 2013, **6**, 1656–1683.

31 C. R. DeBlase, K. Hernandez-Burgos, K. E. Silberstein, G. G. Rodriguez-Calero, R. P. Bisbey, H. D. Abruna and W. R. Dichtel, *ACS Nano*, 2015, **9**, 3178–3183.

32 L. Motiei, Y. Yao, J. Choudhury, H. Yan, T. J. Marks, M. E. van der Boom and A. Facchetti, *J. Am. Chem. Soc.*, 2010, **132**, 12528–12530.

33 F. B. Abdelrazzaq, R. C. Kwong and M. E. Thompson, *J. Am. Chem. Soc.*, 2002, **124**, 4796–4803.

34 S. Shankar, M. Lahav and M. E. van der Boom, *J. Am. Chem. Soc.*, 2015, **137**, 4050–4053.

35 K. Takada, R. Sakamoto, S.-T. Yi, S. Katagiri, T. Kambe and H. Nishihara, *J. Am. Chem. Soc.*, 2015, **137**, 4681–4689.

36 G. de Ruiter and M. E. van der Boom, *Angew. Chem., Int. Ed.*, 2012, **51**, 8598–8601.

37 K. Terada, K. Kanaizuka, V. M. Iyer, M. Sannodo, S. Saito, K. Kobayashi and M. Haga, *Angew. Chem., Int. Ed.*, 2011, **50**, 6287–6291.

38 P. B. Paramonov, S. A. Paniagua, P. J. Hotchkiss, S. C. Jones, N. R. Armstrong, S. R. Marder and J.-L. Bredas, *Chem. Mater.*, 2008, **20**, 5131–5133.

39 M. Chockalingam, N. Darwish, G. Le Saux and J. J. Gooding, *Langmuir*, 2011, **27**, 2545–2552.

40 J. Monot, M. Petit, S. M. Lane, I. Guisle, J. Leger, C. Tellier, D. R. Talham and B. Bujoli, *J. Am. Chem. Soc.*, 2008, **130**, 6243–6251.

41 E. S. Gawalt, G. Lu, S. L. Bernasek and J. Schwartz, *Langmuir*, 1999, **15**, 8929–8933.

42 C. L. Pang, M. Watkins, G. Cabailh, S. Ferrero, L. T. Ngo, Q. Chen, D. S. Humphrey, A. L. Shluger and G. Thornton, *J. Phys. Chem. C*, 2010, **114**, 16983–16988.

43 J. A. Libera, R. W. Gurney, S. T. Nguyen, J. T. Hupp, C. Liu, R. Conley and M. J. Bedzyk, *Langmuir*, 2004, **20**, 8022–8029.

44 A. M. Massari, R. W. Gurney, C. P. Schwartz, S. T. Nguyen and J. T. Hupp, *Langmuir*, 2004, **20**, 4422–4429.

45 H. C. Yang, K. Aoki, H. G. Hong, D. D. Sackett, M. F. Arendt, S. L. Yau, C. M. Bell and T. E. Mallouk, *J. Am. Chem. Soc.*, 1993, **115**, 11855–11862.

46 H. G. Hong, D. D. Sackett and T. E. Mallouk, *Chem. Mater.*, 1991, **3**, 521–527.

47 M. Haga, K. Kobayashi and K. Terada, *Coord. Chem. Rev.*, 2007, **251**, 2688–2701.

48 C. Guang, H. G. Hong and T. E. Mallouk, *Acc. Chem. Res.*, 1992, **25**, 420–427.

49 A. Clearfield, *Chem. Mater.*, 1998, **10**, 2801–2810.

50 Y. Ha, S. Jeong, J. Wu, M.-G. Kim, V. P. Dravid, A. Facchetti and T. J. Marks, *J. Am. Chem. Soc.*, 2010, **132**, 17426–17434.

51 Y. Ha, J. D. Emery, M. J. Bedzyk, H. Usta, A. Facchetti and T. J. Marks, *J. Am. Chem. Soc.*, 2011, **133**, 10239–10250.

52 Y. Ha, K. Everaerts, M. C. Hersam and T. J. Marks, *Acc. Chem. Res.*, 2014, **47**, 1019–1028.

53 N. Tuccitto, V. Ferri, M. Cavazzini, S. Quici, G. Zhavnerko, A. Licciardello and M. A. Rampi, *Nat. Mater.*, 2009, **8**, 41–46.

54 H. Nishihara, K. Kanaizuka, Y. Nishimori and Y. Yamanoi, *Coord. Chem. Rev.*, 2007, **251**, 2674–2687.

55 J. S. Kim, M. Granstrom, R. H. Friend, N. Johansson, W. R. Salaneck, R. Daik, W. J. Feast and F. Cacialli, *J. Appl. Phys.*, 1998, **84**, 6859–6870.

56 C. Picart, J. Mutterer, L. Richert, Y. Luo, G. D. Prestwich, P. Schaaf, J. C. Voegel and P. Lavalle, *Proc. Natl. Acad. Sci. U. S. A.*, 2002, **99**, 12531–12535.

57 P. Lavalle, C. Gergely, F. J. G. Cuisinier, G. Decher, P. Schaaf, J. C. Voegel and C. Picart, *Macromolecules*, 2002, **35**, 4458–4465.

58 C. Porcel, P. Lavalle, V. Ball, G. Decher, B. Senger, J. C. Voegel and P. Schaaf, *Langmuir*, 2006, **22**, 4376–4383.

59 R. A. McAloney, M. Sinyor, V. Dudnik and M. C. Goh, *Langmuir*, 2001, **17**, 6655–6663.

60 B. Schoeler, E. Poptoschev and F. Caruso, *Macromolecules*, 2003, **36**, 5258–5264.

61 D. M. DeLongchamp, M. Kastantin and P. T. Hammond, *Chem. Mater.*, 2003, **15**, 1575–1586.

62 T. Nagashima, T. Nakabayashi, T. Suzuki, K. Kanaizuka, H. Ozawa, Y.-W. Zhong, S. Masaoka, K. Sakai and M. Haga, *Organometallics*, 2014, **33**, 4893–4904.

63 T. Shinomiya, H. Ozawa, Y. Mutoh and M.-a. Haga, *Dalton Trans.*, 2013, **42**, 16166–16175.

64 J. Choudhury, R. Kaminker, L. Motiei, G. de Ruiter, M. Morozov, F. Lupo, A. Gulino and M. E. van der Boom, *J. Am. Chem. Soc.*, 2010, **132**, 9295–9297.

65 C. Agnes, J.-C. Arnault, F. Omnes, B. Jousselme, M. Billon, G. Bidan and P. Mailley, *Phys. Chem. Chem. Phys.*, 2009, **11**, 11647–11654.

66 T. Liu, L. Finn, M. Yu, H. Wang, T. Zhai, X. Lu, Y. Tong and Y. Li, *Nano Lett.*, 2014, **14**, 2522–2527.

67 D. A. Buttry and M. D. Ward, *Chem. Rev.*, 1992, **92**, 1355–1379.

68 A. S. Arico, P. Bruce, B. Scrosati, J. M. Tarascon and W. Van Schalkwijk, *Nat. Mater.*, 2005, **4**, 366–377.

69 S. W. Lee, N. Yabuuchi, B. M. Gallant, S. Chen, B.-S. Kim, P. T. Hammond and Y. Shao-Horn, *Nat. Nanotechnol.*, 2010, **5**, 531–537.

70 H. R. Byon, S. W. Lee, S. Chen, P. T. Hammond and Y. Shao-Horn, *Carbon*, 2011, **49**, 457–467.

71 R. Sakamoto, S. Katagiri, H. Maeda and H. Nishihara, *Coord. Chem. Rev.*, 2013, **257**, 1493–1506.

72 Y. Wang, S. Tao, Y. An, S. Wu and C. Meng, *J. Mater. Chem. A*, 2013, **1**, 8876–8887.

73 J. Zhang and X. S. Zhao, *J. Phys. Chem. C*, 2012, **116**, 5420–5426.

74 H. B. Li, M. H. Yu, F. X. Wang, P. Liu, Y. Liang, J. Xiao, C. X. Wang, Y. X. Tong and G. W. Yang, *Nat. Commun.*, 2013, **4**, 1894.

75 T. N. Ramesh, R. S. Jayashree, P. V. Kamath, S. Rodrigues and A. K. Shukla, *J. Power Sources*, 2002, **104**, 295–298.

76 G. Yu, X. Xie, L. Pan, Z. Bao and Y. Cui, *Nano Energy*, 2013, **2**, 213–234.

77 H. Wang, Y. Liang, T. Mirfakhrai, Z. Chen, H. S. Casalongue and H. Dai, *Nano Res.*, 2011, **4**, 729–736.

78 B. E. Logan, B. Hamelers, R. A. Rozendal, U. Schrroder, J. Keller, S. Freguia, P. Aelterman, W. Verstraete and K. Rabaey, *Environ. Sci. Technol.*, 2006, **40**, 5181–5192.

79 K. Rabaey and W. Verstraete, *Trends Biotechnol.*, 2005, **23**, 291–298.

80 D. R. Bond and D. R. Lovley, *Appl. Environ. Microbiol.*, 2003, **69**, 1548–1555.

81 M. Graetzel, *Acc. Chem. Res.*, 2009, **42**, 1788–1798.

82 F. C. Krebs, *Sol. Energy Mater. Sol. Cells*, 2009, **93**, 394–412.

83 G. Li, V. Shrotriya, J. S. Huang, Y. Yao, T. Moriarty, K. Emery and Y. Yang, *Nat. Mater.*, 2005, **4**, 864–868.

84 J. C. Cuevas and E. Scheer, *Molecular Electronics: An Introduction to Theory and Experiment*, World Scientific, Singapore, 2010.

85 C. Li, A. Mishchenko, I. Pobelov and T. Wandlowski, *Chimia*, 2010, **64**, 383–390.

86 R. Venkatramani, S. Keinan, A. Balaeff and D. N. Beratan, *Coord. Chem. Rev.*, 2011, **255**, 635–648.